Theoretical Study of the Cyclometalated Iridium(III) Complexes Used as Chromophores for Organic Light-Emitting Diodes

Boris Minaev,*,† Valentina Minaeva,‡ and Hans Ågren†

Theoretical Chemistry, Royal Institute of Technology, SE-106 91 Stockholm, Sweden, and Bogdan Khmelnitskij National University, 18031 Cherkassy, Ukraine

Received: August 19, 2008; Revised Manuscript Received: November 12, 2008

Time-dependent density functional theory with linear and quadratic response technology is used to calculate electronic structure, spectra, and spin−orbit coupling effects for analysis of the main mechanism for phosphorescence of the recently synthesized iridium complex [bis(2-phenylpyridine)(2-carboxy-4-dimethylaminopyridine)iridium(III)]. This compound exhibits strong green phosphorescence which is used in solution processable organic light-emitting diode devices (OLEDs) to overcome the efficiency limit imposed by the formation of triplet excitons. Attempting to foresee new structure−property relations that can guide an improved design of OLED devices based on phosphorescence of the lowest triplet state, we have conducted a theoretical analysis of the photophysical properties of a series of iridium cyclometalated complexes.

I. Introduction

Organic light-emitting diodes (OLEDs) and other electroluminescent devices based on iridium cyclometalated complexes have attracted extensive attention because of their potential to achieve a high external quantum efficiency.[1−5] Multilayer OLEDs based on these complexes, prepared via vacuum evaporation or via solution processing, have continuously been analyzed in order to meet the demands of stability, efficiency, and color purity.[3] In that context the solution-processing technique has offered an economic production route of great interest for OLED technology. The main requirement for OLEDs of the next generation is to design efficient phosphorescent dopants to emit sharp colors with very high phosphorescence quantum yields. The common approach to make such dopants is to introduce various electron-withdrawing or electron-donating substituents in the coordinated ligands.[4] In particular, iridium complexes containing large π-conjugated ligands, like 2-phenylpyridine anions (ppy^-), have the advantage that their emission wavelength can be tuned from blue to red by the peripheral substitution of ppy by electron-withdrawing and electron-donating substituents or by replacement of chelating ligands.[1−7]

Success in the development of efficient emitters depends to a great extent on the knowledge of the nature of the emissive excited states. To that end density functional theory (DFT) has been applied to study the electronic effects of different ligands and substituents in the ground and excited states involved in the emission process. Time-dependent (TD) DFT calculations of the iridium cyclometalated complexes for OLED materials have become increasingly popular in recent time[1,2,4,5,8−10] after the pioneering work of Hay on the iridium complexes of the $Ir(ppy)_3$ and $Ir(ppy)_2(acac)$ types, where acac = acetylacetonate.[11] Hay interpreted all low-lying excited states of these compounds as metal-to-ligand charge transfer (MLCT) states. One important issue here is the extent of mixture of ligand-localized (LL) and the MLCT character in the excited states of the cyclometalated complexes.

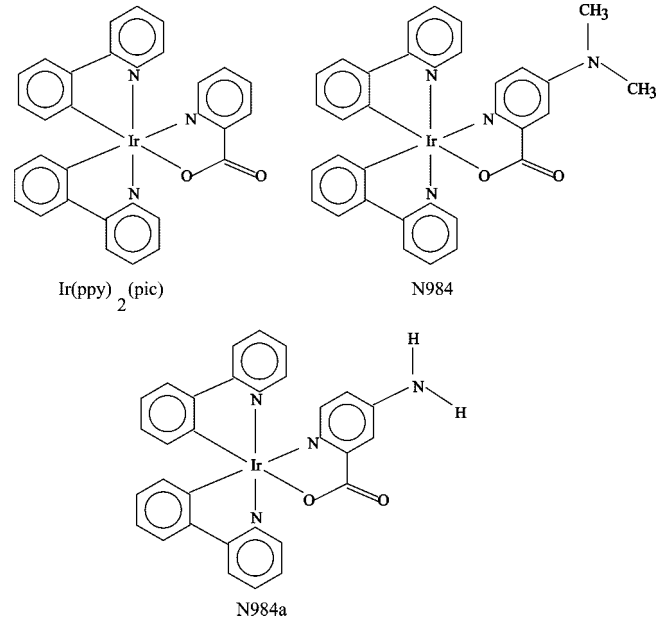

Figure 1. Cyclometalated iridium complexes studied in this work.

Phosphorescent emitters that contain a heavy metal Ir center possess an advantage over pure organic fluorescent emitters because of their strong spin−orbit coupling (SOC) induced by the presence of 5d electrons at the heavy atom. This SOC allows for harvesting both triplet and singlet excitons generated by recombination of charge carriers. Recently, a novel complex, [bis(2-phenylpyridine)(2-carboxy-4-dimethylaminopyridine)iridium(III)] (denoted as N984, see Figure 1), has been synthesized and reported to exhibit a relatively high phosphorescence quantum yield (70 ± 10%) in solution at room temperature and in a solid-state film prepared by dissolving 1% N984 in a PMMA matrix.[3]

Traditional OLEDs are based on organic conjugated polymers as they lend the possibility of creating charge carrier recombination and formation of excitons with high efficiency of light emission.[12] The typical OLED device consists of a multilayer

* To whom correspondence should be addressed.
† Royal Institute of Technology.
‡ Bogdan Khmelnitskij National University.

10.1021/jp807429h CCC: $40.75
Published on Web 01/05/2009

of luminescent organic polymers sandwiched between two metal electrodes. Electrons and holes are first injected from the electrodes into the polymer. These charge carriers migrate through the organic layer and form excitons when the radical pairs of oppositely charged polarons capture each other. Since the charge pairs are nongeminate, they have random spin orientation and the singlet (S) and triplet (T) colliding pairs are therefore equally probable. By statistics the S:T excitons are created with the ratio 1:3, since the triplet state has three spin projections and the singlet has only one microstate. Fluorescence occurs from the S states, whereas the T states are nonemissive in typical organic polymers which do not contain heavy atoms.[12] The phosphorescence from triplet excitons is much less intense since the $T_1 \rightarrow S_0$ transitions in organic polymers are a few orders of magnitude weaker than the spin-allowed $S_1 \rightarrow S_0$ fluorescent transitions. The phosphorescence gains the dipole activity through spin−orbit coupling (SOC) perturbation. SOC is, however, very weak in organic polymers because the orbital angular momentum between spatial parts of the $^3(\pi\pi^*)$ and $^1(\pi\pi^*)$ states of the conjugated chromophores is almost quenched. The absence of heavy elements in the pure organic system is the second important reason for a weak SOC perturbation. Emission from the triplet state has a very low rate constant and cannot compete with nonradiative quenching at room temperature. Consequently, it has been assumed that the quantum yield has an upper statistical limit of 25% in OLEDs based on pure organic polymers.[12] In order to compel the triplet excitons to emit light to compete with nonradiative deactivation and to do useful work in OLEDs, we need to add complexes of heavy elements which will participate in the charge carrier recombination and at the same time provide strong SOC in order to overcome the spin prohibition of the phosphorescent $T_1 \rightarrow S_0$ transition. The above-mentioned cyclometalated photocatalytic complexes of the N984 type fit these conditions quite well.[3]

Like in the $Ir(ppy)_3$ complex,[11] a strong SOC can emerge at the Ir center because of large changes in orbital angular momentum between MLCT states of the S and T types.[10] This SOC induces highly competitive $T_1 \rightarrow S_0$ transition probability and large quantum efficiency of the OLED. At the same time the green color of the N984 phosphorescence (508 nm) is well suited for its use in full color displays.

First-principle theoretical analysis of phosphorescence of organometallic compounds has recently become a realistic proposition with the use of the quadratic response (QR) technique in the framework of the time-dependent DFT approach.[10,13,14] Implementing this method we want in this work to present connections between features of electronic structures and photophysical properties including phosphorescence rates and energy transfer mechanisms of the $T_1 \rightarrow S_0$ transition of the N984 dopant in order to interpret the high efficiency of the corresponding OLED materials.

II. Method of Calculation

The geometrical structures of the N984, N984a, and $Ir(ppy)_2(pic)$ complexes (Figure 1) were optimized for the singlet ground state and for the first excited triplet state at the DFT level of theory using the hybrid exchange-correlation functional of Becke's three-parameter and the Lee−Yang−Parr approximation (B3LYP)[15] and Lanl2DZ basis sets of Hay−Wadt pseudopotentials[16] adopting the Berny optimization algorithm as it is implemented in the Gaussian 03 program.[17] The time-dependent DFT approach is used for calculations of excitation energies and transition moments for S−S transitions with the same approximation. Solvent effects on absorption spectra were calculated in the framework of the polarized continuum model (PCM)[18] with the TD DFT approach.[17] In calculations of SOC and phosphorescence radiative lifetimes, we also used another basis set: the effective core potential (ECP) basis sets of the Stuttgart group (SDD)[19] for the Ir atom and the 6-311G* basis set[20] for the light elements.

The SOC and phosphorescence calculations were performed with the Dalton program[21] for the N984a species by means of the TD DFT approach with quadratic response theory.[14,22] The Einstein coefficient for spontaneous emission (radiative rate constant) A^k from one of the three spin sublevels (denoted by $k = x, y, z$) of the lowest triplet state $|T_1^k\rangle$ in the zero magnetic field (ZMF) and the phosphorescence radiative lifetime τ^k were calculated by the equation

$$A^k = \frac{1}{\tau^k} = \frac{4}{3t_0}\alpha_0^3(\Delta E^k)^3 \sum_{\alpha\in\{x,y,z\}} |M_\alpha^k|^2 \qquad (1)$$

where $t_0 = (4\pi\varepsilon_0)^2\hbar^3/m_e e^4$, α_0 is the fine-structure constant, ΔE^k is the transition energy, and M_α^k is the α-axis projection of the electric dipole transition moment vector between the ground singlet state and the k-spin sublevel of the ZMF triplet state.

This transition moment can be calculated as the residue of a quadratic response function in the framework of the TD DFT approach.[22] In case of the S−T transitions the zeroth-order contribution to the transition moments vanishes due to spin orthogonality. The first and main contribution to the M_α^k value comes from the first-order corrected wave functions. Neglecting spin−spin coupling, the ZMF sublevels of the triplet state are considered to be energy degenerate in the first order, so the final expression reduces to

$$M_\alpha^k = \sum_{n=0}^{\infty} \frac{\langle S_0|\hat{\mu}_\alpha|S_n\rangle\langle S_n|\hat{H}_{SO}|T_1^k\rangle}{E(S_n) - E(T_1)} + \sum_{l}^{x,y,z}\sum_{n=1}^{\infty} \frac{\langle S_0|\hat{H}_{SO}|T_n^l\rangle\langle T_n^l|\hat{\mu}_\alpha|T_1^k\rangle}{E(T_n) - E(S_0)} \qquad (2)$$

where the Cartesian components, T^x, T^y, T^z, with zero projections of the total spin on the corresponding axes[22] are used since we consider the external ZMF case and $\hat{H}_{SO}$ is the SOC operator. It is used here in the effective single-electron approximation.[23] For an effective core potential (ECP) of the iridium atom, this approximation reduces the number of electrons and removes the two-electron SOC integrals, which greatly facilitates the calculations. It has been shown that the parametrized single-electron SOC operator combined with the use of ECPs can give phosphorescence lifetimes that are within 15% of the values obtained by a full relativistic four-component model.[24]

In the high-temperature limit (usually $T \geq 77$ K, when spin−lattice relaxation equalizes sublevels population before emission) the radiative lifetime τ of the triplet state is obtained by averaging over spin sublevels

$$\frac{3}{\tau} = \sum_{k=1}^{3} \frac{1}{\tau_k} \qquad (3)$$

Infrared and nonresonance Raman spectra are calculated for both S_0 and T_1 states at the optimized geometries by Hessian matrix evaluation.[17] All normal modes are found to have real vibrational frequencies; thus, the calculated structures correspond to true global minima on the potential hypersurfaces. Displacements along few normal modes are used for estimation of the SOC integrals, resposible for spin-vibronic perturbations.

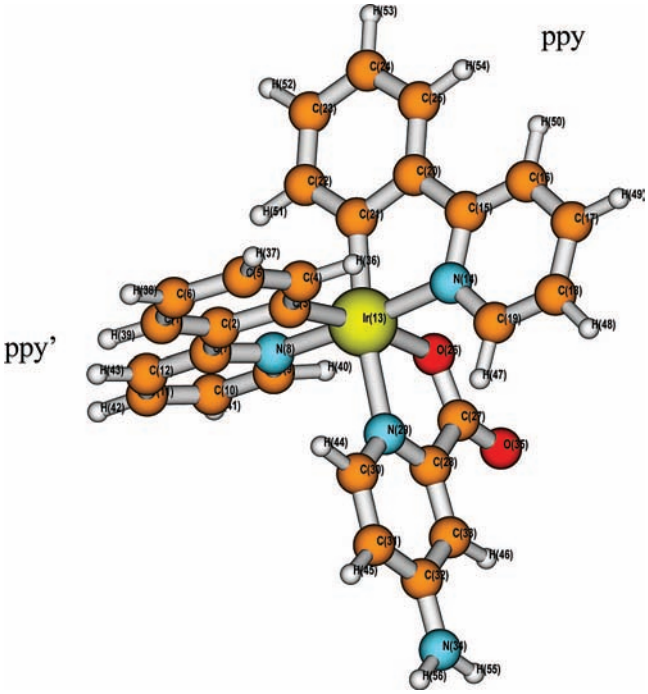

Figure 2. Structure and labeling for the N984a complex.

III. Results and Discussion

A. Structure and Charge Localization. The numeration of atoms for the optimized structure of the [bis(2-phenylpyridine)(2-carboxy-4-aminopyridine)iridium(III)] complex is presented in Figure 2. This complex is used for simulation and denoted as N984a. The dimethylamino derivative (N984 complex) studied by Bolink et al.[3] has a very similar structure as follows from our calculations; the only significant difference is connected with the stretching by 0.007 Å of the $C_{32}-C_{31}$ and $C_{32}-C_{33}$ bonds adjacent to the dimethylamino group. The optimized C−N and C−H bonds length in the dimethylamino group are close to 1.47 and 1.1 Å, respectively. Thus we shall concentrate our attention in the following on the more simple N984a complex taking into account some comments on small effects of methyl groups, if necessary.

First we want to compare the N984a complex with the genuine nonsubstituted $Ir(ppy)_3$ compound which is a benchmark species in the multilayer OLED technology.[10,12,25,26] It is interesting to make a comparison of the studied N984 complex with the earlier calculated structure and phosphorescence properties of the $Ir(ppy)_3$ and $Ir(ppy)_2bpy^+$ complexes (Tables 1, 7).[27,28]

Introduction of the 2-picolinate anion in the $Ir(ppy)_2^+$ residue provides some distortion in comparison with the $Ir(ppy)_3$ complex[10] (Table 1). The links between the iridium ion and the ppy ligands in general get shorter (from 2.15 to 2.05 Å for Ir−N bonds and from 2.035 to 2.014 Å for some Ir−C bonds, Table 1). The changes inside the ppy ligands are minor. The phenylpyridine ligand lying opposite to the Ir−O bond (we call it ppy′) is more perturbed: the $Ir-C_3$ and $Ir-N_8$ bonds in ppy′ are shorter (2.014 and 2.05 Å, respectively) than the corresponding $Ir-C_{21}$ and $Ir-N_{14}$ bonds in the neighboring ppy ligand (2.025 and 2.064 Å, respectively). In the 2-picolinate ligand the Ir−N and Ir−O bonds are quite long (Table 1); thus, they correspond to the weakest metal−ligand coordination valence. For this ligand the coordination bond angle is the small one ($\angle N_{29}-Ir-O_{26} = 76.5°$) in comparison with other ligands (for example, $\angle N_{14}-Ir-C_{21} = 80.5^o$). The amino group is almost coplanar with the picolinate plane (deviation is 0.5°). The dihedral angle $\angle Ir-O_{26}-C_{27}-C_{28} = 177.5°$ is a typical one for all other coordination links. Calculated results are in good agreement with a recent X-ray diffraction measurements.[29] The $Ir-N_{14}$ and $Ir-N_{29}$ bonds are found to be equal to 2.059 and 2.144 Å, respectively,[29] which support our results on the weak coordination of the 2-picolinate ligand (Table 1).

A short comment about the structure of nonsubstituted $Ir(ppy)_3$ benchmark complex should be made in connection with footnote *c* in Table 2; in the ground state of this complex the C−C bond in the ppy moiety between the coordinated carbon atom and the interligand link should be longer than others (the bonds C_2-C_3 and $C_{20}-C_{21}$ in Figure 2 and Table 2). It is the longest bond in the phenyl part of the phenylpyridine molecule itself, and it should be even longer in all Ir(III) complexes containing ppy ligands, because of the asymmetry of the Ir−C (short) and Ir−N (long) distances. Our B3LYP calculations for $Ir(ppy)_2(CN)_2$, $Ir(ppy)_2(bpy)^+$, and similar complexes for Ru(II) support this conclusion. There are also numerous supports from experimental results collected in the Cambridge Crystallographic Data Base.[25,30] That is why rather short lengths of such bonds presented in ref 25 for a number of analyzed molecular arrangements in the $Ir(ppy)_3$ crystal seem to be erroneous.

The Mulliken atomic charge for Ir in both N984 and N984a complexes is equal to +0.93; thus, the Ir(III) ion withdraws about two electrons from three negatively charged ligands. The ppy′ and ppy ligands bear small negative charges (−0.36 and −0.20, respectively), and the picolinate ligand has −0.37 total charge (all charges are in atomic units). The picolinate structure is more close to the neutral picolinic acid charge distribution than to the anion. In this respect the carboxylic bond angle ($\angle O-C-O = 127°$) is only slightly larger than that for the formic acid ($\angle O-C-O = 124.9°$). The total charge of amino group is close to zero (−0.019 in N984 and −0.044 in N984a complexes).

Comparison of the 4-amino-2-picolinate in the N984a complex with the 2-picolinate ligand in the similar $Ir(ppy)_2(pic)$ complex (without NH_2 group) indicates only minor changes in the optimized geometries. The metal−ligand bond lengths deviate by not more than ± 0.001 Å (only the Ir−O bond is shorter in the 2-picolinate ligand by 0.002 Å). The pyridine ring in the 4-amino-2-picolinate moiety exhibits some quinoid character: the $C_{30}-C_{31}$ and $C_{33}-C_{28}$ bond lengths (1.395 and 1.392 Å) are shorter than in the picolinate ligand (1.402 and 1.404 Å), and the $C_{32}-C_{31}$ and $C_{33}-C_{32}$ bond lengths (1.423 and 1.419 Å) are longer than the corresponding picolinate bonds (1.41 and 1.405 Å), respectively. Thus the optimized structures of all three compounds are quite similar in terms of bond lengths and charge distribution, but their energetic parameters are rather different; introduction of donor group (NH_2 and $N(CH_3)_2$ in the N984a and N984 complexes, respectively) in the ancillary picolinate ligand leads to remarkable shift of the LUMO level and corresponding changes in absorption and luminescence properties.

B. Comparison of the S_0 and T_1 States Structure of the [Bis(2-phenylpyridine)(2-carboxy-4-aminopyridine)iridium-(III)] Complex. From the point of view of the OLED phosphorescence properties, we need to compare the optimized structure of the ground singlet (S_0) and the first excited triplet (T_1) states of the N984a dye. From Table 1 one can see that mainly the ppy′ ligand is distorted upon S_0-T_1 transition. The phenylpyridine C−C links are nonequal in two phenylpyridine moieties: the C_2-C_7 bond length is shortened by 0.036 Å upon excitation (from 1.467 until 1.431 Å), while the ppy ligand

TABLE 1: Bond Lengths (Å) for the Ground (S_0) and for the First Excited Triplet State (T_1) of the N984, N984a, and Ir(ppy)$_3$ Complexes

	S_0N984	S_0N984a	S_0Ir(ppy)$_3$			T_1N984a	T_1Ir(ppy)$_3$
bond	calcd	calcd	calcd[a]	exptl[b]	exptl[c]	calcd	calcd[a]
Ir−N_8	2.049	2.050	2.153	2.132	2.086	2.048	2.176
Ir−N_{14}	2.064	2.064	2.153	2.132	2.086	2.076	2.169
Ir−N_{29}	2.174	2.176	2.151	2.132	2.086	2.233	2.116
Ir−C_3	2.015	2.014	2.035	2.024	2.034	1.988	2.000
Ir−C_{21}	2.025	2.025	2.035	2.024	2.034	2.002	2.030
Ir−C_{27}	—	—	2.035	2.024	2.034	—	2.048
Ir−O_{26}	2.188	2.189	—	—	—	2.163	—

[a] Reference 10. [b] Reference 35. [c] Reference 25.

TABLE 2: Bond Lengths (Å) for the Ground (S^0) and the First Triplet Excited State (T_1) of the N984a and the Ir(ppy)$_3$ Complexes[a]

		N984a	N984a	Ir(ppy)$_3$		
ligands	bond	S_0	T_1	S_0	exptl S_0 [b,c]	T_1
ppy	C_2−C_7	1.467	1.431	1.467		1.419
ppy	C_{15}−C_{20}	1.463	1.463	1.467		1.468
pic	C_{27}−C_{28}	1.530	1.524	1.467		1.468
ppy	C_2−C_3	1.435	1.467	1.436	1.391[d] (1.423)	1.485
ppy	C_{20}-C_{21}	1.430	1.435	1.436	1.391[d] (1.423)	1.430
ppy	C_6−C_2	1.414	1.428	1.414		1.427
ppy	C_{23}−C_4	1.413	1.414	1.414		1.415
ppy	C_1−C_6	1.402	1.396	1.400		1.398
ppy	C_{24}−C_{25}	1.401	1.403	1.400		1.404
ppy	C_5−C_4	1.407	1.407	1.406		1.408
ppy	C_{22}−C_{23}	1.406	1.405	1.406		1.406
ppy	C_3−C_4	1.416	1.415	1.419	1.415 (1.405)	1.419
ppy	C_{22}−C_{21}	1.415	1.415	1.419	1.415 (1.405)	1.418
ppy	C_1−C_2	1.415	1.430	1.417		1.432
ppy	C_{20}-C_{25}	1.415	1.413	1.417		1.414
ppy	C_7−N_8	1.383	1.420	1.381	1.378 (1.358)	1.439
ppy	C_{15}−N_{14}	1.384	1.386	1.381	1.378 (1.358)	1.381
ppy	C_9−N_8	1.361	1.363	1.361	1.379 (1.345)	1.361
ppy	C_{19}−N_{14}	1.361	1.360	1.361	1.379 (1.345)	1.361
ppy	C_9−C_{10}	1.399	1.393	1.399		1.392
ppy	C_{19}−C_{18}	1.397	1.397	1.399		1.392
ppy	C_{10}-C_{11}	1.411	1.437	1.411		1.435
ppy	C_{17}−C_{18}	1.411	1.414	1.411		1.413
ppy	C_{12}−C_{11}	1.401	1.389	1.400		1.388
ppy	C_{17}−C_{16}	1.399	1.399	1.400		1.399
ppy	C_7−C_{12}	1.412	1.426	1.416		1.425
ppy	C_{15}−C_{16}	1.413	1.412	1.416		1.412

[a] Ligands notations refer to the former one. [b] Reference 25. [c] Reference 30 (in parentheses). [d] See text.

remains almost unchanged. Among other deformations in the ppy′ ligand, one can see prolongation of the N_8−C_7 bond length by 0.037 Å, the C_2−C_3 bond by 0.032 Å, and the smaller change of the C_2−C_1 bond length from 1.415 to 1.430 Å. The bond C_{10}−C_{11} is stretched by 0.026 Å upon S_0−T_1 excitation. One should also note a short reduction of the C−N bond length in the amino group from 1.381 to 1.379 Å though the ancillary picolinate ligand is not much affected during the $S_0 \rightarrow T_1$ transition. Only the C═O bond is slightly shortened from 1.260 to 1.255 Å with simultaneous extension of the C−O bond length from 1.322 to 1.326 Å. These minor distortions are still important since there are no other indications of the ancillary ligand involvement into the structural changes upon $S_0 \rightarrow T_1$ excitation (see also zero spin density induced by this transition, Table 3).

The metal−ligand interactions are essentially changed in the T_1 state (Table 1). The weak Ir−O bond is getting stronger; its bond length is shortened from 2.189 to 2.163 Å. The Ir−C_3 bond in the ppy′ ligand lying opposite to the Ir−O link is also shortened (from 2.014 to 1.987 Å). Its strength and force constant are unusually high among all studied cyclometalated complexes of iridium(III) ion.[3,10,28] (It is comparable with the Ir−C bond in Ir(ppy)$_2$(acac) complex, where acac = acetoylacetonate.[11,31])

The spin density distribution (Table 3) also indicates that the ppy′ ligand together with the iridium ion are excited in the triplet state and supports an assignment of the $S_0 \rightarrow T_1$ transition as a metal-to-ligand charge transfer (MLCT) with simultaneous excitation in one phenylpiridine moiety. The sum of atomic spin densities in the ppy′ ligand (1.263) together with almost a half of the spin at the Ir center (Table 3) provide spin density (ρ = 1.738) close to 2, the total value for the triplet state. The rest of nonpaired spin density is localized mostly on the phenyl part of the ppy ligand (with essential spin polarization) and on the O_{26} atom of the ancillary ligand (Table 3).

In contrast to the total atomic spin density, an isotropic hyperfine coupling (HFC) constant at the ^{193}Ir isotope is negligible (a_{Ir} = −0.0001 MHz). This is because the spin density at the iridium ion in the T_1 state is concentrated on 5d orbitals, which do not contribute to the Fermi contact isotropic HFC.

TABLE 3: Atomic Spin Density (ρ_N) and Hyperfine Coupling (HFC) Parameters (MHz) of Magnetic Isotopes (N = ^{13}C, ^{14}N, ^{17}O, ^{193}Ir) for the Optimized Geometry of the First Triplet Excited State (T_1) of the N984a Complex, Calculated by the UB3LYP Method[a]

N	ρ_N	a_N	B_{aa}	B_{bb}	B_{cc}	N	ρ_N	a_N	B_{aa}	B_{bb}	B_{cc}
			ppy′						ppy		
C_1	0.058	2.22	−2.05	−1.67	3.72	N_{14}	0.031	0.58	−2.08	−1.62	3.70
C_2	0.145	7.28	−4.67	−4.49	9.16	C_{15}	0.022	0.78	−2.61	−1.35	3.96
C_3	0.175	11.57	−4.92	−4.53	9.45	C_{16}	0.003	−0.28	−0.61	0.01	0.60
C_4	−0.011	−4.27	−0.62	−0.48	1.10	C_{17}	0.020	1.15	−1.78	−1.29	3.07
C_5	0.187	13.18	−5.12	−4.77	9.88	C_{18}	0.031	2.07	−2.47	−1.90	4.37
C_6	0.084	3.68	−2.55	−2.44	4.99	C_{19}	−0.011	−1.16	−1.50	−0.06	1.56
C_7	0.197	12.01	−6.29	−6.08	12.37	C_{20}	0.068	5.59	−5.54	−4.45	9.99
N_8	0.193	7.95	−3.81	−3.62	7.43	C_{21}	−0.026	−8.68	−1.88	0.43	1.45
C_9	−0.065	−9.00	−2.68	0.83	1.85	C_{22}	0.070	4.4	−5.01	−3.97	8.98
C_{10}	0.197	13.65	−5.26	−4.84	10.09	C_{23}	−0.021	−2.84	−1.67	0.50	1.17
C_{11}	0.100	5.50	−2.99	−2.73	5.72	C_{24}	0.081	6.11	−5.99	−5.19	11.17
C_{12}	0.003	−3.08	−0.70	−0.23	0.94	C_{25}	−0.024	−3.05	−2.18	0.80	1.38
Ir_{13}	0.475	0.00	−0.56	0.28	0.28						
			picolinate						picolinate		
O_{26}	0.066	−6.30	10.40	9.57	−19.97	C_{27}	−0.004	−1.23	−1.18	−0.34	1.52
C_{28}	0.003	−0.11	−1.24	0.44	0.80	N_{29}	0.007	4.26	−0.72	−0.53	1.25
C_{30}	0.001	−0.25	−1.37	0.34	1.03	C_{31}	0.001	−0.07	−0.35	0.02	0.33
C_{32}	−0.001	−0.02	−0.46	0.06	0.40	C_{33}	0.002	0.46	−0.37	−0.17	0.54
N_{34}	0.000	−0.02	−0.07	−0.01	0.08	O_{35}	−0.002	0.15	1.41	0.03	−1.44

[a] a_N, isotropic Fermi HFC constants; B_{aa}, anisotropic HFC tensor components (the main axes orientation is available by request).

TABLE 4: Calculated TD DFT Vertical Absorption Spectrum of the N984a Complex in Vacuum

	λ (nm)		f	$\psi_i \rightarrow \psi_j$		
state	exptl[a]	calcd	calcd	TD DFT[b]	character of excitation	orbitality interpretation
T_1	480	509		0.67(125 → 126)	MLCT + L′L	$d_\sigma + \pi_{ppy} \rightarrow \pi^*_{ppy'}$
T_2	—	491		0.66(125 → 127)	MLCT + LL′	$d_\sigma + \pi_{ppy'} \rightarrow \pi^*_{ppy}$
S_1	448	466	0.0243	0.68(125 → 126)	MLCT + L′L	$d_\sigma + \pi_{ppy} \rightarrow \pi^*_{ppy'}$
S_2	448	445	0.0090	0.67(125 → 127)	MLCT + LL′	$d_\sigma + \pi_{ppy'} \rightarrow \pi^*_{ppy}$
S_3	428	432	0.0025	0.67(125 → 128)	MLCT + 2Lpic	$d_\sigma + \pi_{2ppy} \rightarrow \pi^*_{pic}$
S_4	398	396	0.0006	0.67(124 → 126)	MLCT + picL′	$d_\pi + \pi^*_{OO} \rightarrow \pi^*_{ppy'}$
S_5	398	391	0.0076	0.70(125 → 129)	MLCT + 2Lpic	$d_\sigma + \pi_{2ppy} \rightarrow \pi^*_{pic}$
S_6	334sh	374	0.0070	0.63(125 → 130) + 0.28(124 → 127)	MLCT + LL	$d_\sigma + \pi_{2ppy} \rightarrow \pi^*_{2ppy}$
S_7	334sh	367	0.0357	0.44(124 → 127) + 0.42(124 →128)	MLCT + LL	$d_\pi + \pi^*_{OO} \rightarrow \pi^*_{all}$
S_8	334sh	362	0.0094	0.57(125 → 131) − 0.31(124 → 128)	MLCT + L′pic	$d_\sigma + \pi_{ppy'} \rightarrow \pi^*_{pic}$
S_9	334	360	0.0794	0.36(124 → 127) − 0.36(124 → 128)	MLCT + LL	$d_\pi + \pi^*_{OO} \rightarrow \pi^*_{all}$
S_{10}	334	358	0.0185	0.56(123 → 127) + 0.38(123 → 126)	MLCT + LL′	$d_\pi + \pi^*_{picN} \rightarrow \pi^*_{all}$
S_{11}	334	352	0.0257	−0.32(123 → 127) + 0.50(123 → 126)	MLCT + LL′	$d_\pi + \pi^*_{picN} \rightarrow \pi^*_{all}$
S_{12}	334	345	0.0013	0.37(120 → 128) + 0.33(121 → 128)	LL′ + $n\pi^*_{pic}$	$\pi_{ppy} + n_O \rightarrow \pi^*_{all}$
S_{14}	334	336	0.0245	0.50(123 → 128) + 0.37(123 → 129)	MLCT + LL′	$d_\pi + \pi^*_{picN} \rightarrow \pi^*_{all}$
S_{15}	334	329	0.0244	0.58(122 → 126) − 0.18(123 →128)	MLCT + LL′	$\pi_{2ppy} + \pi^*_{picN} \rightarrow \pi^*_{all}$
S_{18}	274sh	315	0.0431	0.60(123 → 129)	MLCT + LL′	$d_\pi + \pi^*_{picN} \rightarrow \pi^*_{all}$
S_{19}	274sh	313	0.0175	0.50(124 → 131) − 0.28(122 → 127)	MLCT + LL	$d_\pi + \pi^*_{OO} \rightarrow \pi^*_{all}$
S_{20}	274sh	310	0.0154	0.62(121 → 126)	LL′	$\pi^*_{ppy'} \rightarrow \pi^*_{ppy}$
S_{24}	274	297	0.0669	0.49(121 → 127) − 0.20(122 → 129)	LL	$\pi^*_{ppy} \rightarrow \pi^*_{ppy}$
S_{26}	274	294	0.0713	0.32(121→ 128) − 0.39(123 → 131)	LL + MLCT	$\pi^*_{picN} \rightarrow \pi^*_{picN}$

[a] Absorption in acetonitrile, ref 3. sh, shoulder. [b] Main contribution to the RPA expansion.

Isotropic HFC constants determined by spin densities at the nuclei (that is, on s atomic orbitals) are relatively large in the ppy and ancillary ligands (Table 3) because their planes are noncoplanar (actually almost perpendicular) to the ppy′ plane. Thus the spin density of the excited triplet $\pi\pi^*$ state of the ppy′ ligand penetrates the σ core of other ligands and produces corresponding isotropic HFC splitting in the EPR spectrum of the T_1 state of all studied complexes. The iridium ion provides such $\pi\sigma$ hyperconjugation between ligands in the excited state of the N984 complex, but the iridium ion itself cannot acquire spin density on the s atomic orbital by specific coordination and 5d AO involvement. This is a general prediction for HFC structure in the EPR spectra of the T_1 state in cyclometalated iridium(III) complexes of similar type. This issue is important for spin−orbit coupling calculation and analysis of the OLED phosphorescence.

Anisotropic HFC tensors for magnetic nuclei of the ppy′ ligand are typical for the excited triplet $\pi\pi^*$ state; the positive components correspond to the c axis (Table 3) which is almost perpendicular ($c \simeq x$) to the plane of the ppy′ ligand. For C_{20}, C_{22}, and C_{24} atoms in the ppy ligand, the c axis is also perpendicular to the corresponding molecular plane ($c \simeq z$). These atoms of the phenyl part of the ppy moiety represent a small alternating chain of $\pi\pi^*$ structure, being the characteristic HFC pattern of the aromatic $^3(\pi\pi^*)$ state. Though the ^{17}O isotope is very difficult for experimental observation in EPR spectra, the calculated HFC tensor for the O_{26} atom is predicted here to be quit interesting; it is strongly anisotropic and corresponds to

TABLE 5: Calculated TD DFT Vertical Absorption Spectrum of the N984a Complex in Acetonitrile Solvent

	λ (nm)		f	$\psi_i \rightarrow \psi_j$		
state	exptl[a]	calcd	calcd	TD DFT[b]	character of excitation	orbitality interpretation
T_1	480	481		0.58(125 → 126) − 0.29(125 → 128)	MLCT + L′L	$d_\sigma + \pi_{ppy} \rightarrow \pi^*_{ppy'}$
T_2	−	491		0.60(125 → 127) + 0.21(125 → 128)	MLCT + LL′	$d_\sigma + \pi_{ppy'} \rightarrow \pi^*_{ppy}$
S_1	448	436	0.0505	0.62(125 → 126) − 0.28(125 → 128)	MLCT + L′L	$d_\sigma + \pi_{ppy} \rightarrow \pi^*_{ppy'}$
S_2	428	424	0.0009	0.63(125 → 127) + 0.27(125 → 128)	MLCT + LL′	$d_\sigma + \pi_{ppy'} \rightarrow \pi^*_{ppy}$
S_3	428	420	0.0016	0.58(125 → 128) + 0.31(125 → 126)	MLCT + 2Lpic	$d_\sigma + \pi_{2ppy} \rightarrow \pi^*_{pic}$
S_4	398	365	0.0019	0.44(124 → 126) − 0.37(123 → 127)	MLCT + picL′	$d_\pi + \pi^*_{OO}\pi^*_{ppy'}$
S_5	398	362	0.0079	0.67(125 → 129)	MLCT + 2Lpic	$d_\sigma + \pi_{2ppy} \rightarrow \pi^*_{pic}$
S_6	334sh	362	0.0163	0.54(123 → 126)	MLCT + LL	$d_\sigma + \pi_{2ppy} \rightarrow \pi^*_{2ppy}$
S_7	334sh	354	0.0592	0.45(124 → 126) + 0.37(124 → 128)	MLCT + LL	$d_\pi + \pi^*_{OO} \rightarrow \pi^*_{all}$
S_8	334sh	353	0.0581	0.42(123 → 127) − 0.32(123 → 126)	MLCT + L′pic	$d_\sigma + \pi_{ppy'} \rightarrow \pi^*_{pic}$
S_9	334	349	0.0253	0.58(125 → 130) − 0.24(123 → 128)	MLCT + LL	$d_\pi + \pi^*_{OO} \rightarrow \pi^*_{all}$
S_{10}	334	348	0.0215	0.33(123 → 127) − 0.50(123 → 126)	MLCT + LL′	$d_\pi + \pi^*_{picN} \rightarrow \pi^*_{all}$
S_{11}	334	344	0.0018	0.39(120 → 128) + 0.34(121 → 128)	LL′ + $n\pi^*_{pic}$	$\pi_{ppy} + n_O \rightarrow \pi^*_{all}$

[a] Absorption in acetonitrile, ref 3. sh, shoulder. [b] Main contribution to the RPA expansion.

TABLE 6: Molecular Orbital Energy Levels (au) and Excited-State Transition Energy (eV) of the $Ir(ppy)_3$, N984, N984a and $Ir(ppy)_2(pic)$ Complexes at the Ground S_0 State Optimized Geometry[a]

	iridium(III) complexes[b]			
molecular orbitals	$Ir(ppy)_3$	N984	N984a	$Ir(ppy)_2(pic)$
LUMO + 2	−0.050(ppy)	−0.049(pic)	−0.053(pic)	−0.060(ppy)
LUMO + 1	−0.050(ppy)	−0.053(ppy)	−0.055(ppy)	−0.064(ppy′)
LUMO	−0.054(ppy)	−0.058(ppy′)	−0.060(ppy′)	−0.072(pic)
HOMO	−0.182(ppy + d_σ)	−0.182(ppy_2 + d_σ)	−0.184(ppy_2 + d_σ)	−0.191(ppy_2 + d_σ)
HOMO − 1	−0.182(ppy + d_π)	−0.202(d_π + π^*_{OO})	−0.205d($_\pi$ + π^*_{OO})	−0.211(d_π + π^*_{OO})
HOMO − 2	−0.182(ppy + d_π)	−0.209(d_π + pic^*_N)	−0.213(d_π + pic^*_N)	−0.224(d_π + pic*)
$E(T_1)$	2.532	2.435	2.436	2.459
$E(S_1)$	2.715(0.005)	2.653(0.024)	2.655(0.024)	2.516(0.003)
$E(S_2)$	2.768(0.002)	2.787(0.011)	2.788(0.009)	2.687(0.025)
$E(S_3)$	2.871(0.002)	2.863(0.004)	2.868(0.003)	2.821(0.009)
$E(S_4)$	2.963(0.024)	3.128(0.004)	3.132(0.001)	3.03(0.006)

[a] Main contributions are given in parentheses. [b] N984 = $Ir(ppy)_2$(2-carboxy-4-dimethylaminopyridine); N984a = $Ir(ppy)_2$(2-carboxy-4-aminopyridine); $Ir(ppy)_2(pic)$ = $Ir(ppy)_2$(2-carboxy-4-pyridine); (ppy) = (2-phenylpyridine).

the $n\pi^*$ character with the charge transfer from the oxygen O_{26} atom to the ppy′ ligand.

Isotropic HFC constants for protons (not shown in Table 3) are relatively large only in the ppy′ ligand. The largest a_H constants are for H_{41} and H_{37} protons (−7.31 and −7.07 MHz, respectively), and for H_{38} and H_{42} atoms they are equal to −3.54 and −4.3 MHz, respectively. Neither amino group nor methylamino group exhibits notable HFC splitting. Nevertheless, these groups influence the visible absorption and emission spectra as it is discussed below in terms of the LUMO level shift.

C. Electronic UV−Visible Absorption Spectra and Solvent Effects. Calculated spectra of both complexes, N984a and N984, are practically identical but differ from the spectrum of the [bis(2-phenylpyridine)(2-carboxy-4-pyridine)iridium(III)] complex. This picolinic acid analogue is denoted as $Ir(ppy)_2(pic)$ in the following.

TD DFT calculations at the optimized ground-state geometry provide vertical excitations in good agreement with the UV−visible absorption spectrum of the N984 complex measured in acetonitrile solution.[3] In the visible region three weak absorption bands are observed at 480, 448, and 428 nm (the former is a weak shoulder). They are interpreted tentatively as the MLCT transitions.[3] Absorptions displayed in the UV region with increasing intensity (weak bands at 398 and 334 nm and strong bands at 274 and 208 nm) are assigned to intraligand $\pi-\pi^*$ excitations.[3]

Our TD DFT calculation supports these assignments in general, but some details should be specified as the following, summarized in Tables 4 and 5. While calculations in vacuum (Table 4) provide only minor agreement with the experimental absorption spectrum measured in acetonitrile solution,[3] the TD DFT calculation in the framework of the PCM model for the CH_3CN solvent gives very good improvement and almost quantitative agreement with observed bands wavelength in the visible region (Table 5).

We have assigned the very weak band at 480 nm to the S−T absorption; its intensity[3] is in qualitative agreement with the oscillator strength (f = 0.0014) calculated by the quadratic response TD DFT method. We have assigned the more intense band at 448 nm to the first S−S transition, which corresponds mostly to the HOMO−LUMO excitation and has a large MLCT character. In Tables 4 and 5, the d_π and d_σ orbitals on the iridium ion are classified with respect to the 4-amino(-2-picolinate) plane; the notation of π_{ppy} orbital refers (as usual) to those MOs which change sign with respect to the corresponding ppy plane.

The HOMO (125, Figure 3) is delocalized on the phenyl π orbitals of both ppy and ppy′ ligands with a large contribution (46%) from the $5d_\sigma$ AO of Ir ion and a minor one (8%) from the $n(O_{26})$ lone pair orbital. The LUMO (126) is localized mostly on the ppy′ ligand and has a strong bonding character for the C_2-C_7 phenylpyridine link. Thus the vertical HOMO → LUMO excitation includes besides the MLCT character also a large dose of interligand $\pi_{ppy} \rightarrow \pi^*_{ppy'}$ excitation.

Vertical transitions from the ground S_0 state to the T_1 and S_1 states in TD DFT treatment have very similar orbital presentations (Table 4). After the relaxation these excited states are rather different in terms of structure and density distribution, but still

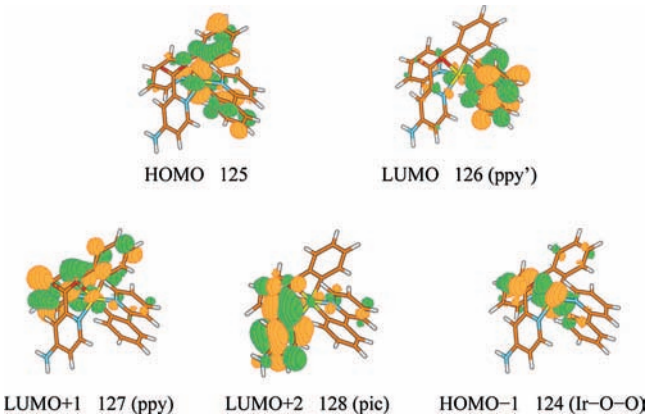

Figure 3. Highest occupied, lowest unoccupied, and some other molecular orbitals of the N984a complex. The LUMO is mostly localized at the ppy′ ligand; the HOMO − 1 (124 orbital) is localized at the Ir ion and carboxy group.

they are highly nonsymmetrical with respect to the ppy and ppy′ ligands. Since LUMO is a $\pi^*_{ppy'}$ orbital with bonding character for the phenylpyridine C−C link, the HOMO → LUMO excitation (Table 4) leads to a strong distortion in the ppy′ ligand with a shortening of the C_2-C_7 bond length and with other distortions in this excited moiety (atomic numbers 1−12 in Tables 2 and 3). This is in agreement with the results of the T_1 state geometry optimization which are discussed below in connection with spin density and HFC parameters. The energy gain after relaxation in the T_1 state is not large (only 0.043 eV or 1 kcal/mol), but the structural changes are quite significant.

From our calculations a dipole moment of the ground state of the N984a complex in vacuum is predicted to be equal to 8.6 D, while in the toluene, CH_2Cl_2, and CH_3CN solvents the dipole moment is changed to 10.2, 11.7, and 12.4 D, respectively. This mutual solvent−solute polarization in the PCM model leads to stabilization of the HOMO energy from −0.184 au in vacuum to −0.188, −0.193, and −0.195 au in the same series of solvents, respectively. Since the energy of the LUMO level is not affected so much, the total blue shift is obtained in all solvents. At the same time the HOMO structure is preserved, but an increasing contribution of the pic ligand is induced in the LUMO by solvents. The first S_0-S_1 transition intensity increases with the rise of the polarity of solvent; the oscillator strength changes from 0.024 to 0.045, 0.051, and 0.052 in the series.

The weak visible absorption at 428 nm is attributed to two quasidegenerate transitions from HOMO to LUMO + 1 and to LUMO + 2, which are strongly mixed upon the influence of solvent (Table 5). The LUMO + 1 function (Figure 3) is a π orbital localized entirely on the ppy ligand. The LUMO + 2 function (Figure 3) represents the π MO of the pic ligand. The absorption band at 428 nm produced mostly by the HOMO → LUMO + 2 transition (125 → 128) has a complicated nature; it includes small MLCT and dd contributions and a large part of the interligand ppy_2 → picolinate excitation (Figures 2 and 3, Table 4). Involvement of the amino group in the upper MO 128 (Figure 3) makes this transition dependent on the nature of ancillary ligand. Indeed this band is not observed in the $Ir(ppy)_2(pic)$ complex,[6] which does not contain the amino group. Other comparisons of absorption spectra of this complex and N984 species indicate some differences in those bands with shorter wavelength which involve the picolinate MOs.

The third S−S transition at 398 nm is strongly affected by solvent (Table 4 and 5). This band can be connected with excitations from MO 124 (Figure 3), which includes the highly polarizable π_{OO^*} orbital on oxygen atoms of the carboxylate group and is strongly stabilized by solvents. Intense transition (125 → 129) also contribute to the band at 398 nm (Table 4). The MO 129 is delocalized on π^* orbitals of all ligands (mostly on pyridine parts); thus, this transition includes charge transfer to the pic ligand with some MLCT character (and with phenylpyridine CT) being the object of a strong solvatochromic effect.

Intense absorption bands in the UV region (274 and 208 nm) are assigned to local $\pi \rightarrow \pi^*$ excitations in the ligands. But in the intermediate region (398−334 nm) we have calculated a great number of excited singlet states with a mixed MLCT and ligand-to-ligand charge-transfer (LL′) character (Tables 4 and 5); many of these S−S transitions are overlapped by more intense intraligand $\pi \rightarrow \pi^*$ absorption bands.

Thus the main trends in vertical absorption spectra of N984 and N984a complexes, including the orbital nature of excited states, solvent effects, and the influence of dimethylamino and amino groups on the spectrum of the $Ir(ppy)_2(pic)$ complex are well understood and explained in our TD DFT calculations.

D. Comparison of Molecular Orbitals and Absorption Spectra of N984, N984a, and $Ir(ppy)_2(pic)$ Complexes. At this point we need to make a more detailed comparison of the N984, N984a, and $Ir(ppy)_2(pic)$ complexes, where pic is picolinate ancillary ligand (without amino group). Molecular orbitals of N984a complex are not changed much upon methylation of the amino group (Table 6, Figure 4). Only HOMO − 2 and LUMO + 2 orbitals, which represent the π MO of the picolinate ancillary ligand, have some small energy shifts, because they involve the π_N AO of the amino group. A negligibly small contribution of methyl hydrogen atoms from dimethylamino group occurs in the HOMO − 2 orbital of the N984 dye.

A remarkable change of MO energy levels occurs in the $Ir(ppy)_2(pic)$ complex. In the absence of amino group the antibonding π MO of picolinate ligand shifts down and becomes the LUMO with relatively low energy (Table 6, Figure 4). The LUMO gets lower by 0.38 eV (0.014 au) in comparison with the N984 complex. This is in agreement with the cyclic voltammogram of the N984 complex, which shows a reversible couple at 0.61 V versus ferrocene Cp_2Fe/Cp_2Fe^+ redox couple due to the Ir(III/IV) reduction−oxidation cycle;[3] upon scanning cathodically the authors of ref 3 observed a reversible reduction wave at −2.55 V versus ferrocene, which is assigned to the reduction of the phenylpyridine by comparison with analogous $Ir(ppy)_3$ and $Ir(ppy)_2(acac)$ complexes. This reduction potential demonstrates that the LUMO is located on the 2-phenylpyridine ligand (ppy′ as follows from our calculations) rather than on aminopicolinate ancillary ligand whose lowest unoccupied MO is destabilized by the presence of the 4-amino group (Table 6) and even more destabilized by the presence of the 4-dimethylamino group.

At the same time, the oxidation potential of the N984 dye is shifted cathodically by 0.1 V compared to the $Ir(ppy)_2(pic)$ complex due to destabilization of the HOMO,[3] which consists mostly of iridium 5d AO (48%) and phenyl parts of both ppy ligands (Figure 2). Although neither amino group nor dimethylamino group enters this HOMO, its energy is destabilized by 0.17 and 0.23 eV in N984a and N984 dyes, respectively, in comparison with the $Ir(ppy)_2(pic)$ complex (Table 6). The $2p_\sigma$ lone pair orbital on oxygen O_{26} atom enters this HOMO (Figure 3) in all three complexes and probably provides an inductive polarization effect of the amino group through the σ core.

TABLE 7: Radiative Phosphorescence Lifetimes for the Three Spin Sublevels τ^{α} (μs) of $Ir(bpy)_2(ppy)^{2+}$, $Ir(ppy)_3$, $Ir(bpy)_3^{3+}$, and N984a Complexes Calculated with the B3LYP QR Method Using Various Basis Sets[a]

molecule	ΔE_{S-T}	τ^x	τ^y	τ^z	τ	τ(exptl)
N984a	2.44(2.44)[b]	3.43	1.58	20.16	3.08	2.42[b]
$Ir(ppy)_3$	2.52(2.42)[c]	1.32	1.32	82.74	1.96	2.0[c]
$Ir(bpy)_3^{3+}$	2.70(2.75)[d]	54.34	54.3	88.01	62.28	54[d]
$Ir(ppy)_2(bpy)^+$	2.14(2.25)[e]	14.32	1.63	162.8	4.83	4.4−5.2[e]

[a] SDD has been used on Ir and 6-31G* on other atoms in all calculations. τ (μs) is the radiative phosphorescence lifetime in the high-temperature limit. ΔE_{S-T} (eV) is the S_0-T_1 excitation energy. Calculations have been performed at the S_0 optimized geometry. [b] Observed in PMMA film; ref 3. [c] Observed in THF at 130 K; ref 26. [d] Reference 36. [e] Observed in 4:1 ethanol:methanol glass at 77 K; ref 27.

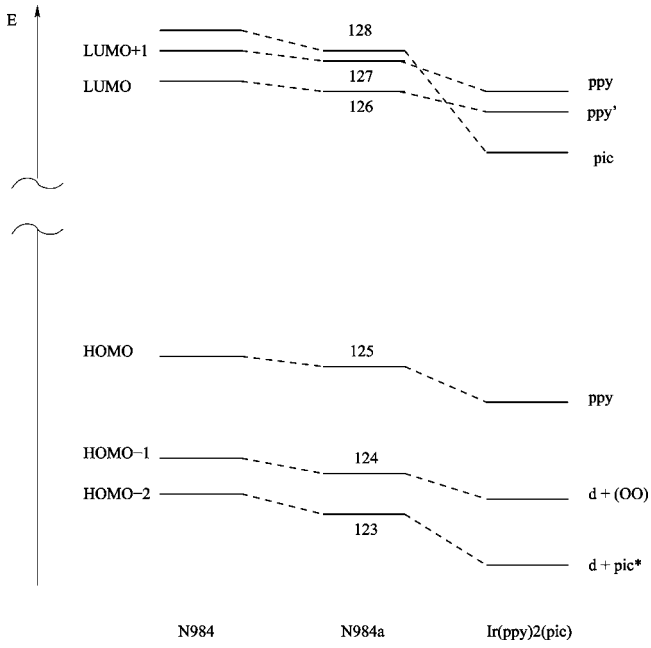

Figure 4. Correlation scheme of molecular orbital energy levels.

In general the three HOMOs and LUMOs levels in the $Ir(ppy)_2(pic)$ complex are much lower than those of the N984 and N984a dyes (Table 6, Figure 4). This is probably due to the low location of the HOMO level of the picolinic acid itself (−0.272 au = −7.4 eV) and to the fact that the picolinate ligand weakly donates to the formation of HOMO of the $Ir(ppy)_2(pic)$ complex during complexation. The increase of HOMO energy in N984 and $Ir(ppy)_3$ dyes (Table 6) makes it possible for easy electron transfer to the host molecules or electron-transporting material. In OLED materials electrons are relatively depleted, and so to balance the number of electrons and holes in the emitting layer, the total number of electrons has to be increased.[9] The HOMO of N984a (and N984) dye is very similar in energy to that of the $Ir(ppy)_3$ complex because it does not contain the pic ligand contributions (Figure 3).

The changes of MO energy levels determine the differences in UV−vis absorption spectra induced by the insertion of amino group in the 4-position of picolinate ancillary ligand (Table 6, Figure 4). The first S_0-S_1 transition has a new orbital nature in the $Ir(ppy)_2(pic)$ complex; this is HOMO−LUMO transition mostly; thus, it represents MLCT to the pic ligand and also the interligand charge transfer to the picolinate moiety. The second, S_0-S_2, transition in the $Ir(ppy)_2(pic)$ complex is more intense and determines the first absorption band of moderate absorbency ($\log \varepsilon = 3.75$, where ε is an extinction coefficient)[6] at 440 nm, which overlaps the weak S_0-S_1 band. Thus this transition exhibits a blue shift (8 nm) with respect to N984 dye which has a notable absorption at 448 nm in similar solvent.[3] The calculated blue shift in vacuum is equal to 466 − 460 = 7 nm, and the same shift is calculated between both complexes in acetonitrile and dichloromethane.

E. Phosphorescence of the $Ir(ppy)_2$(2-carboxy-4-aminopyridine) Complex. The nature of the lowest triplet T_1 state in cyclometalated iridium(III) complexes with the ppy ligands including mixed $Ir(ppy)_2(bpy)^+$, N984, and N984a complexes is quite similar. This is the HOMO−LUMO excitation which represents the MLCT state with a large admixture of interligand (ppy)−(ppy′) excitations. For this reason the calculated radiative properties of their phosphorescence are also similar (Table 7). Each spin sublevel provides its own lifetime and polarization for the T_1-S_0 transition (Table 7), but these data are not available from room temperature phosphorescence measurements.[10,26] The calculated radiative lifetime of the N984a complex in the high-temperature limit (3.08 s) is in good agreement with the phosphorescence radiative lifetime (2.42 s) measured for N984 dopant in polymethylmethacrylate film.[3]

In the $Ir(ppy)_2(pic)$ complex the nature of the lowest triplet T_1 state is rather different. The random phase approximation (RPA) in the TD DFT approach provides the following orbital excitations in the T_1 state expansion: 0.53(121 → 123) + 0.41(121 → 122), where 121 and 122 orbitals are HOMO and LUMO, respectively. Thus the charge transfers to both the ppy and pic ligands are present. The T_1 state in the $Ir(ppy)_2(pic)$ complex is more delocalized than in the N984 complex, where the ancillary ligand is not much involved in the $T_1 \rightarrow S_0$ transition.

Thus introduction of the dimethylamino group (or a simple amino group) in the 2-pyridinecarboxylate (picolinate) part of the N984 complex leads to a shift of the LUMO level from the weakly bound (pic) ancillary ligand to the strongly bound cyclometalating phenylpyridine (ppy′) moiety in agreement with proposal of Bolink et al.[3] Introducing the donor amino group into picolinate, we return the N984 dye to the family of strongly phosphorescent cyclometalated iridium(III) compounds of the $Ir(ppy)_3$ type with all peculiarities of their intersystem crossing (ISC) and emission processes discussed before.[10]

Fast ISC together with short radiative lifetime provide a high phosphorescence quantum yield of such a family of compounds, because the SOC matrix elements between low-lying singlet states and the T_1 triplet are very large like in $Ir(ppy)_3$ dye.[10] All these states include large contributions of the MLCT character with $5d_\sigma$ and $5d_\pi$ orbital involvement (Tables 6, 4); thus, great changes of the orbital angular momentum at the Ir center and strong SOC matrix elements emerge between them.

In the $Ir(ppy)_2(pic)$ complex the second triplet T_2 state is almost degenerate with the T_1 triplet and has a similar expansion: −0.42(121 → 123) + 0.56(121 → 122). Both "in-phase" and "out-of-phase" resonance structures with charge transfer to ppy′ and pic ligands are delocalized and serve as an indication of the Jahn−Teller effect.[10] The wave functions of these two low-

lying triplet states are also very different from the corresponding singlet excited-state orbital structure in terms of the RPA expansion.

One can anticipate that spin-vibronic mixing between low-lying singlet and triplet states, responsible for the ISC process, would be inefficient because of delocalization and quasidegeneracy of two low-lying triplet states. In the N984 complex, localization of the T_1 excited state on one ppy′ ligand provides the high SOC matrix elements like in the $Ir(ppy)_3$ dye[10] and efficient spin-vibronic coupling induced by local vibrations in the ligand and in the Ir−C bond. For this reason the quantum yield of phosphorescence (Φ_p) of the $Ir(ppy)_2(pic)$ complex is much lower (0.033)[6] than Φ_p of the N984 dye (0.70 ± 0.1) in similar solvents at room temperature.[3]

In contrast to the $Ir(ppy)_2(pic)$ dye, the intersystem crossing $S_k \rightarrow T_1$ in the N984a complex is very fast. The SOC matrix elements $<S_k|H_{so}|T_1>$ are very large for higher excited singlet states $k = 7, 9-11$ (Table 4). All these states include a large contribution from the different types of $5d_\pi$ orbitals; thus, they include a strong change of the orbital angular momentum at the metal center. All these active singlet states are also close in energy and can participate in the ISC process and in vibronic mixing. Comparison with the SOC integrals at the triplet-state geometry indicates their strong dependence on the Ir−C distortion and on the intraligand displacements. Such spin-vibronic interaction can induce electronic energy transfer to vibrational movement, which is necessary for efficient $S_k \rightarrow T_1$ ISC process.[10,13,34] The phenylpyridine C−C link together with Ir−C and Ir−N bonds arrange a coordinative cycle. All bonds in this cycle are strongly deformed upon $T_1 \rightarrow S_0$ transition; thus, the breathing vibrations are the most important as they determine spin-vibronic perturbation between S and T states. These vibrations in the ground and triplet states have similar frequency about of 1330 cm^{-1} since they are mixed with the in-plane C−C−H deformations as follows from our calculation. This vibration should be active in spin-vibronic coupling and provide the intense 0−1 fundamental band in the phosphorescence emission. A similar feature is observed in the wide band of green emission of the N984 complex in solvent and in the electroluminescent spectrum of OLED devices containing this dye. The emission spectrum of a solid-state film prepared by dissolving 1% N984 dye in a PMMA matrix shows maxima at 506 nm with a distinct shoulder at 535 nm similar to the phosphorescence of solution.[3] We assign this shoulder to vibronic transition of the mode mentioned above.

The main difference in the phosphorescence quantum yield from the $Ir(ppy)_2$ (pic) and N984 complexes can be explained also by their difference in the nonradiative quenching of the triplet state $T_1 \rightarrow S_0$. The HOMO and LUMO in the $Ir(ppy)_2(pic)$ complex have appreciable contributions from $5d_1$ and $5d_2$ orbitals, respectively. This leads to nonzero SOC matrix elements $\langle S_0|H_{so}|T_1\rangle = 68$ cm^{-1}, which induce nonradiative quenching of the triplet state $T_1 \rightarrow S_0$. In the N984a dye this integral is much lower (12 cm^{-1}). Since the square of the SOC matrix element determines the rate of the $T_1 \rightarrow S_0$ nonradiative quenching, this rate should be much slower in the N984 complex and the phosphorescence quantum yield should be higher than in the $Ir(ppy)_2(pic)$ complex.

It should be natural to calculate τ at the T_1 state optimized geometry, but since the final state is the ground state which determines vibronic structure of the emission spectrum it is useful to consider the $T_1 \rightarrow S_0$ transition probability at the S_0 optimized geometry. From our previous experience,[10,13] it follows that the τ calculations at the T_1 state optimized geometry do not provide new useful information on the phosphorescence spectra. The influence of the inhomogeneous environment on phosphorescence and zero-field splitting is well-known for organic molecules and heterocycles;[32,33] it could be essential for the presently studied complexes. We are planing to study the solvent effect on T_1 state emission of the N984 dye in the near future.

IV. Conclusion

Geometry and electronic structure of series of amino derivatives of the [bis(2-phenylpyridine)(2-carboxypyridine)iridium(III)] compounds (denoted as $Ir(ppy)_2(pic)$ complexes) have been calculated in the ground singlet and first excited triplet states by density functional theory (DFT). Linear and quadratic time-dependent DFT has been employed for the absorption spectra and the phosphorescence radiative lifetimes (τ) of the [bis(2-phenylpyridine)(2-carboxy-4-aminopyridine)iridium(III)] complex, which simulates the green-emitting N984 dye ([bis(2-phenylpyridine)-(2-carboxy-4-dimethylaminopyridine)iridium(III)] compound) synthesized recently and utilized in a very efficient multilayer OLED.

Our TD DFT calculations elucidate the mechanism of strong electroluminescence of the studied dye by identifying the origin of the triplet-state emission of the $Ir(ppy)_3$, $Ir(bpy)_3^{3+}$, and $Ir(ppy)_2(bpy)^+$ complexes (bpy = bipyridine) of the comparable N984a dye. It is shown that the dimethylamino group provides similar properties as the simulating amino group in the absorption and phosphorescence spectra. The molecular orbitals of the N984 and N984a dyes and of the $Ir(ppy)_2(pic)$ complex are discussed together with the solvent effect on their absorption spectra in the framework of the polarizable continuum model. A large blue shift in acetonirile solvent (27 nm) in comparison with calculation in vacuum provides good agreement with the observed spectrum of the N984 complex in solution.

The calculated lifetime is compared with the previously studied *fac*-tris(2-phenylpyridine)iridium(III) complex [$Ir(ppy)_3$] and similar dyes. Since the ancillary picolinate (pic) ligand is not much involved into the S_0-T_1 transition of the N984 dye (which is indicated by spin density and optimized structures), the calculated τ value does not differ significantly from the phosphorescence radiative lifetime of the benchmark $Ir(ppy)_3$ complex.

Comparison of molecular orbitals of the N984 and $Ir(ppy)_2(pic)$ compounds indicates that introduction of the amnio group into the fourth position of the picolinate ligand provides a distinct change in the nature of the LUMO level; from being localized on the picolinate moiety in the $Ir(ppy)_2(pic)$ complex the LUMO level is shifted to phenylpyridine (ppy′) ligand in the N984 complex. Because of this LUMO shift, the nature of the lowest triplet state is also changed resulting in the highly phosphorescent N984 dye in comparison with low quantum yield emission from the $Ir(ppy)_2(pic)$ complex.

It is found that the orbital structure of the T_1 state of the N984 dye is similar to the structure of the tris(iridium(III)) complexes; it means that their triplet states have a localized character with the $T_1 \rightarrow S_0$ transition being determined mostly by charge transfer from one of the ppy ligands to the metal; interligand charge transfer is also present in this strong electroluminescence. By this reason electron−hole recombination (EHL) in the OLED devices fabricated by utilizing N984, which is blended with the large band gap polymer (poly-*N*-vinylcarbazole), is highly effective: different ligands strongly interact with the polymer environment and produces a trapped T_1 exciton during the EHL process.

The phosphorescence lifetime in the high-temperature limit is found to be in reasonable agreement with experimental data

measured in a solid polymer matrix and in degassed acetonitrile solution. Thus we can hope that the essential features of such a complicated phenomenon like phosphorescence of green-emitting complex N984 and its blends with polymers in OLED devices are truly interpreted by means of Kohn−Scham time-dependent density functional theory. Further studies of spin-vibronic coupling and intermolecular interactions with the polymer surroundings will give deeper insight in parameter design for iridium cyclometalated complexes as efficient phosphorescence dopants in electroluminescent devices.

Acknowledgment. This work was supported by the Visby project "Education and Research Network in Light Emitting Diode Materials" funded by the Swedish Institute (project code no. 01403/2007) and also by the Ukrainian−Romanian project "Design of sensitizing dyes for solar cells based on nanocrystaling TiO_2". Helpful discussions with Olav Vahtras and Mihai Girtu are greatly acknowledged.

References and Notes

(1) Nazeeruddin, M.; Wegh, R.; Zhou, Z.; Klein, C.; Wang, Q.; Angelis, F. D.; Fantacci, S.; Grätzel, M. *Inorg. Chem.* **2006**, *45*, 9245.

(2) Angelis, F. D.; Fantacci, S.; Evans, N.; Klein, C.; Zakeeruddin, S.; Moser, J.; Kalyanasundaram, K.; Bolink, H.; Grätzel, M.; Nazeeruddin, M. *Inorg. Chem.* **2007**, *46*, 5989.

(3) Bolink, H.; Coronado, E.; Santamaria, S.; Sessolo, M.; Evans, N.; Klein, C.; Baranoff, E.; Kalyanasundaram, K.; Grätzel, M.; Nazeeruddin, M. *Chem. Commun.* **2007**, 3276.

(4) Censo, D. D.; Fantacci, S.; Angelis, F. D.; Evans, N.; Klein, C.; Kalyanasundaram, K.; Bolink, H.; Grätzel, M.; Nazeeruddin, M. *Inorg. Chem.* **2008**, *47*, 980.

(5) Avilov, I.; Minoofar, P.; Cornil, J.; Cola, L. D. *J. Am. Chem. Soc.* **2007**, *129*, 8247.

(6) Xu, M.; Zhou, R.; Wang, G.; Xiao, Q.; Du, W.; Che, G. *Inorg. Chim. Acta* **2008**, *361*, 2407.

(7) Slinker, J.; Gorodetsky, A.; Lowry, M.; Wang, J.; Parker, S.; Rohl, R.; Bernhard, S.; Malliaras, G. *J. Am. Chem. Soc.* **2004**, *126*, 2763.

(8) Nozaki, K. *J. Chin. Chem. Soc.* **2006**, *53*, 101.

(9) Park, N.; Choi, G.; Lee, Y.; Kim, Y. *Curr. Appl. Phys.* **2006**, *6*, 620.

(10) Jansson, E.; Minaev, B.; Schrader, S.; Ågren, H. *Chem. Phys.* **2007**, *333*, 157.

(11) Hay, P. *J. Phys. Chem. A* **2002**, *106*, 1634.

(12) Baldo, M.; O'Brien, D.; You, Y.; Shoustikov, A.; Sibley, S.; Thompson, M.; Forrest, S. *Nature* **1998**, *395*, 151.

(13) Minaev, B.; Ågren, H. *Chem. Phys.* **2005**, *315*, 215.

(14) Tunnell, I.; Rinkevicius, Z.; Salek, P.; Vahtras, O.; Helgaker, T.; Ågren, H. *J. Chem. Phys.* **2003**, *119*, 11024.

(15) Becke, A. *J. Chem. Phys.* **1993**, *98*, 5648.

(16) Hay, P.; Wadt, W. J. *Chem. Phys.* **198582**, 299.

(17) Frisch, M. J.; Trucks, G. W.; Schlegel, H. B.; Scuseria, G. E.; Robb, M. A.; Cheeseman, J. R.; Montgomery, J. A., Jr.; Vreven, T.; Kudin, K. N.; Burant, J. C.; et al. *Gaussian 03, Revision C.02*; Gaussian, Inc.: Wallingford, CT, 2004.

(18) Miertus, S.; Tomasi, J. *Chem. Phys.* **1982**, *65*, 239.

(19) Andrae, M.; Haeussermann, U.; Dolg, M.; Stoll, H.; Preuss, H. *Theor. Chim. Acta* **1990**, *77*, 123.

(20) Hehre, W.; Ditchfield, R.; Pople, J. *J. Chem. Phys.* **1972**, *56*, 2257.

(21) Helgaker, T.; Jensen, H. J. A.; Jørgensen, P.; Olsen, J.; Ruud, K.; Ågren, H.; Andersen, T.; Bak, K. L;. Bakken, V.; Christiansen, O.; et al. 2001.

(22) Minaev, B.; Tunnell, I.; Salek, P.; Loboda, O.; Vahtras, O.; Ågren, H. *Mol. Phys.* **2004**, *102*, 1391.

(23) Koseki, S.; Schmidt, M.; Gordon, M. *J. Phys. Chem. A* **1998**, *102*, 10430.

(24) Jansson, E.; Norman, P.; Minaev, B.; Ågren, H. *J. Chem. Phys.* **2006**, *124*, 114106.

(25) Breu, J.; Stossel, P.; Schrader, S.; Starukhin, A.; Finkenzeller, W.; Yersin, H. *Chem. Mater.* **2005**, *17*, 1745.

(26) Finkenzeller, W.; Yersin, H. *Chem. Phys. Lett.* **2003**, *377*, 299.

(27) Garces, F.; King, K.; Watts, R. *Inorg. Chem.* **1988**, *27*, 3464.

(28) Minaev, B.; Ågren, H.; Angelis, F. D. *Chem. Phys.*, in press.

(29) Baranoff, E.; Suarez, S.; Bugnon, P.; Barolo, C.; Buscaino, R.; Scopelliti, R.; Zuppiroli, L.; Grätzel, M.; Nazeeruddin, M. *Inorg. Chem.* **2008**, *47*, 6575.

(30) Allen, F.; Kennard, O. *Chem. Des. Autom. News* **1993**, *8*, 31.

(31) Lamansky, S.; Djurovich, P.; Murphy, D.; Abdelrazzaq, F.; Kwong, R.; Tsyba, I.; Bortz, M.; Mui, B.; Bau, R.; Thompson, M. *Inorg. Chem.* **2001**, *40*, 1704.

(32) Minaev, B.; Loboda, O.; Vahtras, O.; Ruud, K.; Ågren, H. *Theor. Chim. Acta* **2003**, *109*, 44.

(33) Loboda, O.; Minaev, B.; Vahtras, O.; Ågren, H.; Ruud, K. *J. Phys. Chem.* **2003**, *119*, 3120.

(34) Macak, P.; Luo, Y.; Ågren, H. *Chem. Phys. Lett.* **2000**, *330*, 447.

(35) Garcs, F.; Dedeiam, K.; Keder, N.; Watts, R. J. *Acta Crystallogr., Sect. C* **1993**, *49*, 1117.

(36) Krausz, E.; Higgins, J.; Reizen, H. *Inorg. Chem.* **1993**, *32*, 4053.

JP807429H